Chapter 3

Data Acquisition and DFC Processing

3.1 Introduction

This chapter presents the acquisition process of vibration signals and the detailed description of the dataset characteristics. Since the rotor faults are more sensitive to vibration data, the referred datasets use different vibration sensors to collect data at different speed, load and other working conditions. To analyze rotor faults other than broken rotor bar fault, more than 80.0% of the works depend on rotor testbeds for faulty data generation. The primary dataset (DS-1) is a novel one which has been collected from a rotor kit setup (Meggitt-Mi 19003) [183], which simulates the real plant varying speed working environment. In addition, a publically available data set called Machinery Fault Database (MaFaulDa) [184] is employed as the second dataset (DS-2) for general performance comparison in the proposed frameworks. The experimental setup, fault simulation process, related parameters of data acquisition, etc., are explained along with the testbed description is given in the first section of the chapter. The remaining sections bring out the significance of DFC in SRF diagnosis in detail to provide an insight into the effective fault diagnosis. Then the section contains the

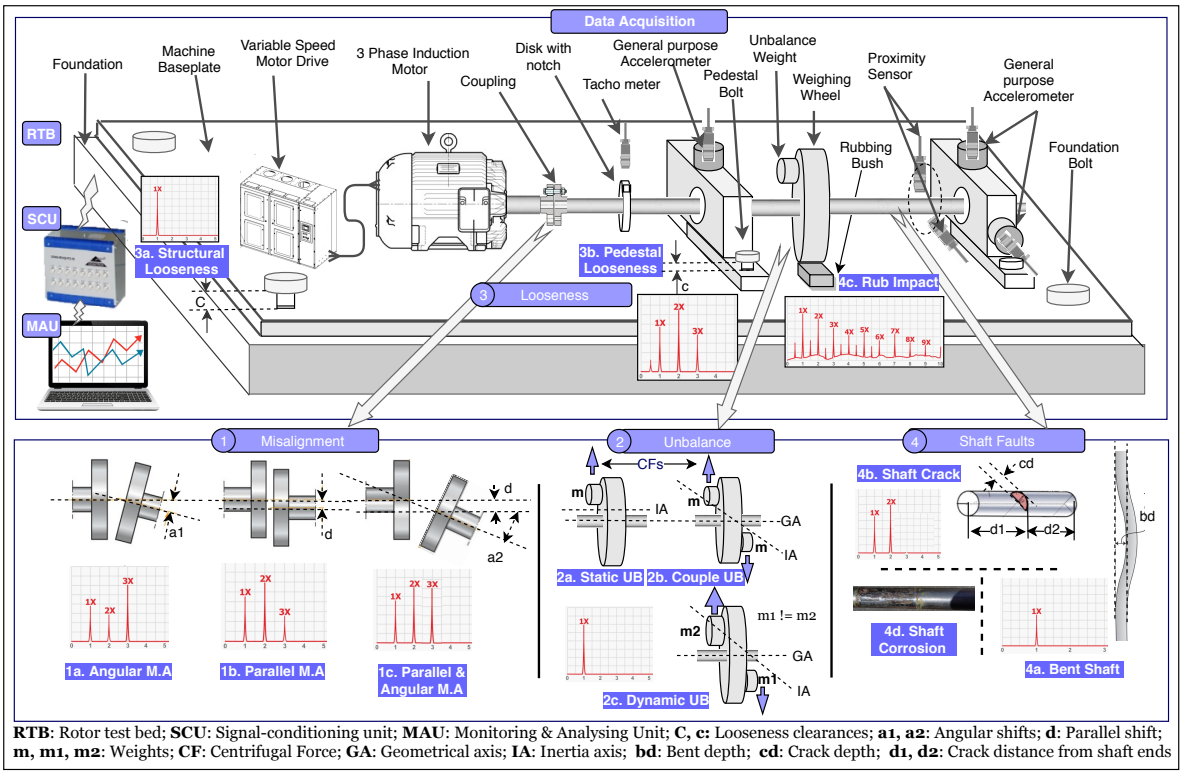

Figure 3.1: Rotor fault implementation in a testbed

proposed DFC extraction process from varying operating conditions followed by the description of the experiment conducted to signify the dominance of DFC as the decision parameter in SRF diagnosis.

3.2 Datasets Description

3.2.1 Meggitt dataset (DS-1)

The data acquisition setup contains the RTB, the signal-conditioning unit (SCU), and the monitoring and analyzing unit (MAU) [16]. Fig. 3.1 presents a diagrammatic representation of a typical rotor testbed-based data acquisition setup along with the fault implementation and the associated frequency responses.

The main component of the testbed assembly is an electric motor controlled by a variable frequency drive (VFD, which varies the frequency and voltage supply) con-

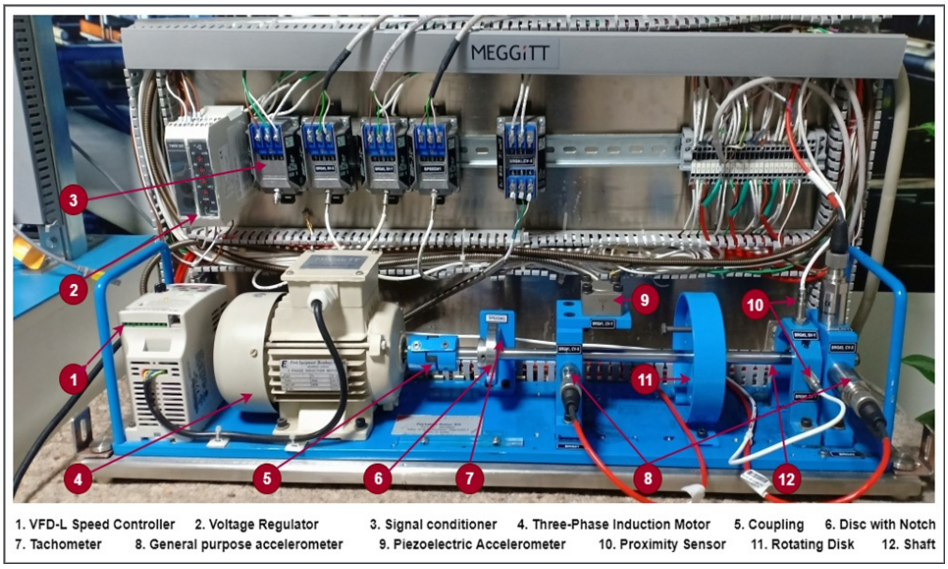

Figure 3.2: Meggitt testbed (Meggitt-Mi 19003)

Table 3.1: Setup conditions for testbed of DS-1 dataset.

Features	**Specification / values**
Sensors	Accelerometer: Piezo-electric , Proximity sensors: Eddy current based
RPM / Frequency	RPM Range: $0 - 3600$ Sampling Frequency: 1 KHz
Motor Power	1 kW-h
Rotor Speeds	750 rpm, 1500 rpm, 2250 rpm, 3000 rpm, 3250 rpm with Runup and Rundown
Unbalance weights	13.0 g and 26.0 g (Dynamic UB)
Diameter	Weighing Disc: 100.18 mm and Shaft:12.66 mm

nected to a rotating shaft via a flexible coupling. The shaft is supported by bearing housing that is fixed by pedestal bolts to the testbed base. The bearing housing has provisions for mounting sensors in horizontal, vertical, and axial directions. The shaft will be mounted with discs for various purposes. Generally, a disc with one or more notches is closely placed with a tachometer that senses the rotational speed of the shaft. This tachometer reference, along with a sensor waveform, is used to calculate the phase

information. Meanwhile, weighing discs, which will likely incorporate grooves, holes, or another eccentric weight connecting provision, will also be mounted on the shafts. The majority of the testbeds are equipped with a metal bush connecting facility to create the rub impact [185]. Contact type general-purpose accelerometers and non-contact type proximity sensors are commonly used for the vibration data acquisition. The acquired data is then passed through an SCU, which often performs signal amplification and analog-to-digital conversion. It is then applied to the MAU, which is generally a computer that carries out the monitoring and analysis of the input signal and any associated tasks with the help of specifically developed software. In SRF, the unbalance

Table 3.2: Setup conditions for testbed of DS-2 dataset.

Features	**Specification / values**
Sensors	Analog tachometer, accelerometers, and microphone.
Frequency RPM	Sampling Frequency: 51.2 kHz RPM Range: $700 - 3600$ rpm
Motor Power	1/4 CV DC
Rotor Speeds	$10.0 - 60.0$ Hz
Unbalance weights	6.0 g, 10.0 g, 15.0 g, 20.0 g, 25.0 g, 30.0 g, 35.0 g
Misalignment	Horizontal: 0.50 mm, 1.0 mm, 1.50 mm, 2.0 mm Vertical: 0.51 mm, 0.63 mm, 1.40 mm, 1.90 mm, 1.27 mm, 1.78 mm
Diameter	Rotor: 152.4 mm and Shaft: 16.0 mm

fault is created by connecting weights (bolts, nuts, washers, etc.) on the weighing disc. Two equal weights are placed 180° apart to create couple unbalance, while a one-sided weight is positioned to generate static unbalance. Much like in couple unbalance, if unequal weights are set in place, then dynamic unbalance can be simulated [26]. The coupling is loosened to induce a parallel shift and/or angular shift to create parallel and/or angular misalignment [185]. In terms of loosening faults, the majority of the works deal with pedestal loosening, which is simulated by loosening the pedestal bolt of

the bearing housing to create clearance from the testbed base [16]. Meanwhile, structural looseness can be demonstrated by loosening the bolt connecting the testbed base to the foundation. The stationary bush that is in contact with the shaft or disc periphery will induce rub impact [26]. The shaft bend and shaft crack provisions are also shown in Fig. 3.1. Here, the experiment is conducted by setting different fault conditions as described before, and then the testbed is set to different rotational frequencies and load conditions to collect data via repeated trials. The SRF dataset created for our experiments consists of six different fault classes namely healthy (HL), static UB (S_UB), couple UB (C_UB), dynamic UB (D_UB), misalignment (MA) and looseness (LS). The data collection conditions and the general testbed information are provided in Table 3.1.

3.2.2 MaFaulDa dataset (DS-2)

MaFaulDa is a publicaly available dataset that uses SpectraQuest's machinery fault simulator and produces multivariate TS data for SRF diagnosis. The dataset uses the two sets of accelerometers for the collection of vibration data, which are organized in three orthogonal directions, i.e., axial, radial, and tangential. It is equipped with a tachometer to measure the system rotation frequency and a microphone to capture the operating sound. The faulty conditions considered in this setup are normal (NM), unbalance (UB), and horizontal misalignment (H_MA) and vertical misalignment (V_MA). The unbalance conditions are simulated with seven different weights. The misalignments are implemented with varying shift clearances in the data gathering process. A total of 1951 various conditions are incorporated in the dataset. For each scenario, the data is collected at 50 kHz over a time interval of 5 seconds, with eight prescribed signals. The MaFaulDa data acquisition setup description is given in Table 3.2.

Table 3.3: Description of rotor faults

Fault Category (Fault No.)			Vibration Characteristics			Assoc. Faults	Cause & Effect
			Plane	Symptomatic Frequency	Phase		
Strucural Rotor Faults	Misalignment (1)	**Angular (1a)**	Axl	2x peaks are higher than 1x peak. Stronger 3x axial and torsional responses at 1/3rd of critical speed.	A phase shift of 180° in the axial direction.	4a(C), Brg. Flts(E)	Cause: Component expansion and cold alignment due to thermal distortions. Improper coupling alignment, Uneven foundation, imparted forces from other components, bent shaft, mass unbalance, etc. Effect: Early fatigue failure, excessive heat and friction, and component damage.
		Parallel (1b)	Rad	2x peaks are higher than 1x peak. Stronger 1x axial and torsional responses.	A phase shift of 180° in the radial direction.		
		Parallel & Angular (1c)	Axl & Rad	2x peaks are higher than 1x peaks. Presence of 3x harmonics.	A phase shift of 180° in radial and axial position		
	Unbalance (2)	**Static (2a)**	Rad	Larger 1x and harmonics with less than 15.0% of the 1x.	A phase shift of 0° in radial direction	4a(C), 3a(C), 4d(C)	Cause: Rotor mass eccentricity due to assembly errors, manufacturing defects, debris deposit, etc. Presence of other faults: bow shaft, corrosion, falling of damaged rotor part, etc. Effect: Higher dynamic load and early fatigue failure, wobbling movement.
		Couple (2b)	Rad	Larger 1x and harmonics with less than 15.0% of the 1x.	A phase shift of 180° in radial direction		
		Dynamic (2c)	Rad	Larger 1x and harmonics with less than 15.0% of the 1x.	0° to 180° Phase shift.		
	Looseness (3)	**Component (3a)**	Axl & Rad	Dominating 2x. Presence of 1x to 10x harmonics, subharmonics (x/2, x/3, etc.), multiples of subharmonics (2x/3, 4x/3, etc.).	Unstable phase reading.	3 (E), 2 (E)	Cause: Improper fittings, tear and wear, thermal expansion. Effect: Damage or detach of components, Secondary faults like misalignment and unbalance.
		Structural (3b)	Rad	Higher 1x and/or 2x. Harmonics frequency amplitude above 50.0% of 1x.	180° phase shift between base plate and foundation	2 (C)	Cause: Loosened bolts or bedplates, deteriorated concrete foundation, loose or distorted machine mountings. Effect: Component looseness, unbalance, and misalignment.
Shaft Faults (4)		**Bent Shaft (4a)**	Axl & Rad	Higher 1x when bent at the middle of shaft. 2x generated when bent close to the coupling.	A phase shift of 180° in the axial & 0° in the radial directions.	2a(E)	Cause: 1) Permanent: Large unbalance force, uneven shrink fittings, residual stress or collision. 2) Temporary: Friction and thermal distortion, high length to width ratio. Effect: Higher dynamic load and early fatigue failure, unbalance.
		Shaft Crack (4b)	Rad	Dominating 2x. Presence of 1x and certain subharmonics (1/2x, 1/x, etc.).	Directly proportional to the depth of the crack.	4c(E), 4a(E)	Cause: Severe thermal and mechanical stresses or manufacturing defects. Effect: Reduction in bending stiffness, shaft bow.
		Rub Impact Fault (4c)	Rad	Higher 1x with 2x, 3x and other harmonics. Presence of 1/2x, 1/3x, etc.	Inconsistent phase.	1 (C), 2 (C), 4a(E)	Cause: Excessive unbalance, misalignment, self-excited instability, resonance, thermal distortions. Effect: Excessive heat, Thermal bow.
		Shaft Corrosion & Wear (4d)	Not directly evident.			4b(E)	Cause: Electrochemical reaction due to environmental factors. Effect: Metal lose, crack
Broken Rotor Bar (5)			Rad	Case 1: Higher 1x with, up to 4x. Pole-pass sidebands with 2x line frequency. Case2: Higher 1x with 2x line frequency sidebands.	Inconsistent phase.	4a(E), 2 (E)	Cause: Thermal, magnetic, dynamic, mechanical, and environmental stresses. Effects: Uneven current flow. Thermal bow and unbalance.

***Abbreviations-** Axl: Axial, Rad: Radial, Assoc.: Associated, Brg. Flts: Bearing Faults, C: Cause of, E: Effect

3.3 DFC and SRF

The study of symptomatic parameters of rotor faults revealed that SRF is more sensitive to DFC of rotational frequency. Hence this section addresses the SRF-DFC correlation and the experiments conducted to substantiate it. The impact of DFC in characterizing the vibration of SRF can be visually verified from Fig 3.3, where DFC representation of a healthy and unbalance vibration signal at 1500 RPM is shown. At the 1x frequency of around 25Hz, the amplitude of unbalance signal is high, and small spikes are present at all the other rotational frequencies. In contrast, for healthy data signal all amplitudes of rotational frequencies are similar. This evidence that DFC can be the clear indicator of SRF. A more detailed description of SRF is given in Table 3.3 with amplitude and phase characteristics, along with the most affected plane, associated faults, and the causes and effects of the faults. The fault-wise description of the impact of DFC in SRF is given below:

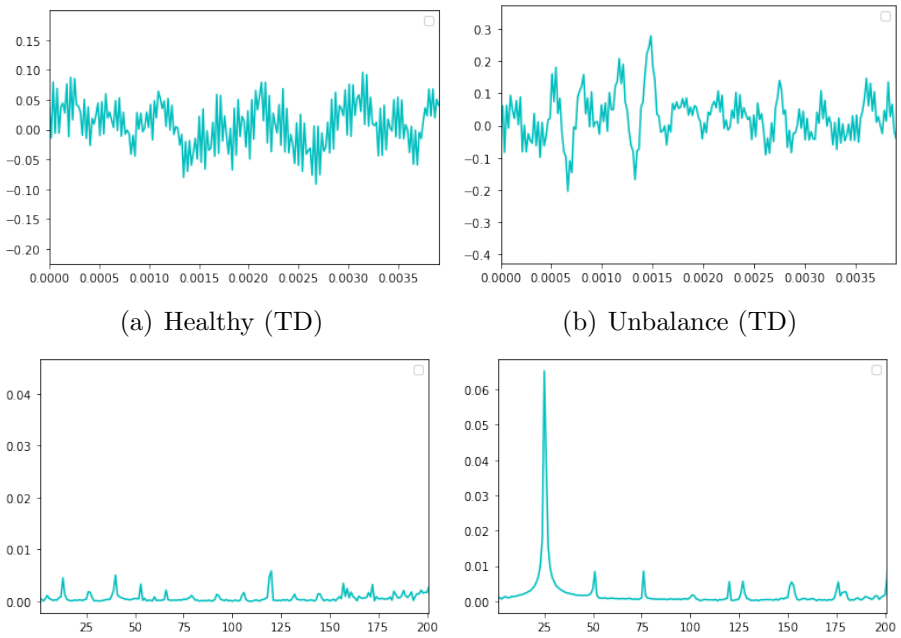

(a) Healthy (TD) (b) Unbalance (TD)

(c) Healthy (DFC) (d) Unbalance (DFC)

Figure 3.3: DFC representation of signal at 1500 RPM

3.3.1 Structural rotor faults

The SRF, being the primary cause of vibration, strongly reflects the abnormal vibrations by various DFC parameters. The vibrational characteristics of faults such as misalignment, unbalance, and looseness are explained in this section to depict the DFC-SRF correlation.

3.3.1.1 Misalignment

Misalignment can be analyzed by comparing the ratio between 1x (unbalance indicator) and 2x (misalignment indicator) components. In normal misalignment scenarios, 2x and 1x components are present in the radial vibration spectrum, with 2x being the predominant component with a range up to 150.0% of 1x [67]. The severe misalignment conditions are characterized by the harmonics 3x to 8x or even a full high-frequency harmonics series. Patel et al. [186] presented certain observations to identify the type of misalignment as well as to distinguish between misalignment and crack faults in the rotor. In order to uniquely identify misalignments, they suggested investigating the presence of strong negative higher harmonic frequency components compared to that of rotor crack. They also observed that stronger 1x axial as well as torsional responses and weak higher harmonics represent parallel misalignment. They added that a strong 3x harmonic component in its axial and torsional vibration response at $1/3^{rd}$ critical speed indicates angular misalignments. Phase information is also used as a defining feature of misalignments. Across the coupling or machine, a phase shift of 180° in the axial position shows angular misalignment, and the same in radial position indicates parallel misalignment, whereas that in both axial and radial position represents combined misalignment [68]. The vibration waveforms follow a periodic pattern having one or two cycles in each revolution of the shaft.

3.3.1.2 Unbalance

The vibration wave produced by unbalance is sinusoidal and occurs at a frequency of 'one per revolution' (1x), i.e., a single frequency vibration with the same amplitude in all radial directions. Other than the severe faulty states, vibration generally contains 1x only, without any harmonics of it. The 1x with high amplitude and its harmonics with less than 15.0% of the 1x is an indication of an unbalanced state [187]. In this case, up to the first critical speed of the machine, the amplitude increases with speed, and the phase from the vertical and horizontal measurements differ by 90°. In dynamic unbalance, there will be 180° phase shift in the radial direction, while static unbalance shows a phase shift of 0°. For unbalance due to the bent shaft, the phase shift of 180° happens in the axial direction with no phase shift in the radial direction [67].

3.3.1.3 Looseness

In the case of component looseness, the initial stage vibration signature contains mostly 1x and 2x components, but with escalated deterioration, the fractional harmonics with increased amplitude starts to appear. Generally, looseness is characterized by several running speed frequency harmonics (1x – 10x) with subharmonics (x/2, x/3, etc.) and their integer multiples (2x/3, 4x/3, etc.) of magnitudes greater than 20.0% of the 1x amplitude. Structural looseness creates 1x and/or 2x radial components with predominant vertical amplitude, subject to the type of issue. For rigidly connected machines with no belts or couplings, the radial 2x signifies looseness. The waveform generated is periodic with one or two cycles per revolution. A phase difference of 180° exists between the foundation and vibrating components in case of structural looseness [67].

3.3.2 Shaft faults

According to the fault categorization from the vibration perspective, the shaft faults such as bending, cracking, and rub impacts are the secondary cause of abnormal vibration. Hence, their frequency characteristic responses are described in this section.

3.3.2.1 Bent shaft

In the case of bent shaft, if the bent is close to the middle of the shaft length, then 1x will be dominating, and 2x will be dominant for the bents near to the couplings. The most affected plane is axial, though vertical and horizontal planes will also give out 1x and 2x peaks [72]. The 2x amplitude can vary from 30.0% of the 1x amplitude to 100.0% – 200.0% of the 1x amplitude. The spectrum of bent shaft is almost similar to that of misalignment; hence, the phase can be used as a good differentiating indicator. In bent shafts, the radial phase measurements will be in phase, while axial measurements will be 180° out of phase at opposite ends of the component [67].

3.3.2.2 Shaft crack

The first and foremost effect of shaft crack is the reduction in bending stiffness in the direction of the crack, which results in inducing excessive 2x vibration in the shaft [71]. The second effect is the rotor bow, where the bending results in the natural axis shift corresponding to the direction of the crack. This effect generates 1x components, which will progressively add to the already existing residual unbalance frequency component [72]. The cracked shaft vibration mostly affects the radial plane, and it produces increased 1x vibration along with the 2x and 3x harmonics. In certain scenarios, the presence of subharmonics 1/2x, 1/x, etc., are also observed with this fault. Studies revealed that the phase shift is directly proportional to the depth of the crack [71, 188].

3.3.2.3 Rub impact

The vibration changes in characteristic ways whenever the rub happens between stationary and non-stationary components. So other than the times there is no contact, the waveform seems absolutely normal. The spectrum will be containing higher amplitude subharmonics and superharmonics of the synchronous frequency with a strong rub impact. Chu et al. [189] observed the presence of 1/2 fractional harmonic components and 1/3 fractional harmonic components along with the 2x, 3x harmonic components. Meanwhile, the existence of pseudo-resonance and backward whirling components showed by [190] as the effect of rub. The phase information shows that it can not maintain a consistent phase in rub related vibration motion.

3.3.3 Broken rotor bar

Uneven current flow to induction motor rotor owing to crack or break results in two kinds of vibration changes. In the first case, 1x and harmonics generally up to 4x will accompany with pole-pass sidebands with quite low 2x line frequency [67]. In the second case, the amplitude of rotor bar passing frequency (RBF, which is the number of rotor bars times the running speed) will be higher, with 2x line frequency sidebands (100Hz or 120Hz) [66]. Due to the motion of vibration, the phase will be consistent in broken rotor bar faults.

3.4 DFC Extraction

According to the literature review, the utilization of DFC is instrumental in developing solutions of SRF. Meanwhile, the literature study upholds the need of more realistic industrial data with varying speed and load conditions, which in turn makes the DFC extraction more complicatied. Hence we proposed the following procedure in DFC extraction and data subsampled feature space creation, which suppresses the other

raw data related issues. Sub-sampling is performed by selecting the summary interval points that ensure sufficient data points in each sensor segment. This stipulates proper extraction of DFC (FD component) and TD representatives of each segment. The process is described as follows:

Let K be the number of sensors mounted at different positions, producing univariate TS vibration signals $V = [V_1, V_2, ..., V_K]$ with each $V_i \in \mathbb{R}^L$ where L is the length of one sample sequence. Since the framework deals with rotational data, one complete informative segment should consider at least the number of sampling points produced in a single rotation. This decision is based on the given rotational frequency in rpm R_s and the sensing frequency S_f of the data acquisition system. The rotation frequency is converted in seconds for the convenience of calculation by $R_f = R_s/60$. Then, the number of sampling points per rotation is calculated by: $S_r = 60S_f/R_s$ or S_f/R_f. Thus, the interval points or segment length is decided according to the condition: $S_o \leq S_r \leq S_l$, where S_o is the overlapping points in segmentation and S_l is the segment length. The segments are extracted equally from all the sensors so that the number of segments from an L length single sensor sequence is:

$$n_s = (L - S_l)/(S_l - S_o) + 1 \tag{3.1}$$

Hence, the segments of sensor S_i are denoted by $V_i = [V_{i,1}, V_{i,1}, ..., V_{i,n_s}]$.

After the segmentation, each segment is depicted by a high-level representation in the sub-sampled feature space. The rotational frequency and its higher-order harmonic components are more sensitive to the SRF. Thus, the basic task is to extract these components from the vibration spectrum. In a real plant scenario, RM working at a fixed rpm (R_s) undergoes speed fluctuations due to varying voltage, connected load, the influence of other rotating components, etc. As a result, the rotational frequency and its harmonic components can not be estimated directly by R_f and its multiples to extract DFC. In faulty conditions, this phenomena of fluctuation of actual values

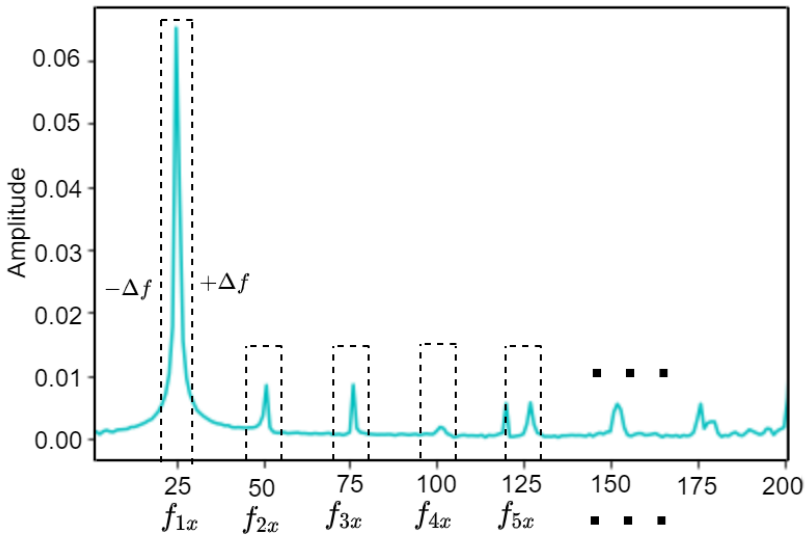

Figure 3.4: DFC extraction from varying RPM

around the theoretical values are more obvious. Hence, the process of extracting DFC with FFT is assisted with proper normalization process [16] to reduce the rate difference under varying operating conditions. This operation is shown as

$$A_{\text{amp}} = \frac{1}{f_n}\sum_{\text{i=1}}^{f_n} amp(f_{ix}) \tag{3.2}$$

$$\mu\left(f_{ix}\right) = \frac{\text{amp}(f_{ix})}{\text{A}_{\text{amp}}}\,(i = 1, 2, ..., f_n) \tag{3.3}$$

Here, we consider f_n frequency bands for DFC extraction and the $amp(f_{ix})$ represents the amplitude corresponding to f_{ix} frequency. The A_{amp} shows the mean of these amplitudes, and finally $\mu(f_{ix})$ gives the normalized amplitude values. There is often a fluctuation observed in the frequency range near the rotation frequency bands, and hence, a multi-pass filter with a frequency range of Δf that extracts frequency between $f_{ix}-\Delta f$ and $f_{ix}+\Delta f$ is used. This has been shown in Fig. 3.4, considering the frequency spectrum of the unbalance fault at 1500 rpm. In practical data collection experiments, it is observed that the rpm variation is approximately less than 10.0%, which doesn't

cause significant amplitude change. Both amplitude and phase values are extracted to generate the DFC components. Similarly, the TD representative of each segment is generated from the data bins of length S_r. The DFC extraction is performed on the harmonic frequencies according to the number of features required, and appended along with the TD features to generate a subsampled vector for representing a particular sensor segment.

3.5 Role of DFC in SRF Diagnosis

This section proves the significance of DFC in SRF diagnosis by comparing the performance of the conventional TD and FD features against DFC features. This study is conducted in order to substantiate DFC as the symptomatic fault feature of SRF. The two top performing ML algorithms, SVM and ANN along with ANFIS algorithm for evaluating fuzzy reasoning on DFC decision parameters are used for the DFC performance comparison. The first two models are the most widely used ML technique in RM fault diagnosis [10]. At the same time, ANFIS blends the ability of fuzzy logic to mimic human reasoning and backpropagation learning of ANN. All three models were tested with ten features each from TD, FD, and DFC features for performance comparison. The TD features contain mean, standard deviation, variance, root mean square, absolute maximum, coefficient of skewness, kurtosis, crest factor, margin factor, and shape factor. The FD features include mean, variance, third moment, fourth moment, grand mean, C factor, D factor, E factor, G factor, and H factor derived from the frequency transformed domain. DFC is represented by amplitude and phase representatives of 1x to 5x frequencies.

ANFIS method was developed by Jang in 1993 [111]. ANFIS model allows user interference compared to ANN which can be utilized to incorporate domain specific decision making criterias. It is a hybrid learning a structure that combines fuzzy logic and ANN which consists of backpropagation learning. But in ANFIS, the fuzzy logic is

Table 3.4: DFC Performance with ML Models

ML Models	DS-1			DS-2		
	TD	FD	DFC	TD	FD	DFC
ANN	84.84	92.49	94.27	87.52	92.76	94.43
SVM	80.51	92.04	93.96	86.07	92.00	94.39
ANFIS	84.46	93.20	95.01	88.52	93.59	95.64

treated more systematically that it demands least expert knowledge. So in this implementation, eventhough it is possible to add the rules related to SRF diagnosis directly, the system is let to learn the rules itself, providing the decision making parameters as input. ANFIS normally has five layers of neurons of which neurons in the same layer are of the same function family. The layers are named as the fuzzification layer (I), the rule layer (II), the normalization layer (III), the defuzzification layer (IV), and the output layer (V). The ANFIS algorithm uses Sugeno based fuzzy logic to deal with imprecision or uncertainty and neural network for adaptability. Integrating the relatively low learning rate neural network with fuzzy logic makes it suitable for time critical applications [191]. SVM is implemented with RBF kernel, and its regularization parameter C is set to 1.0, and the parameter γ that decides the influence of training example is set to 0.1 by performing grid search. The ANN has three layers, i.e., the input layer contains ten nodes, the hidden layer with non-linear RBF activation function containing 20 nodes, and the output layer nodes decided depending on the number of classes.

The results are shown in Table 3.4, from which it is observed that TD features show the least accuracy on both datasets as they are extracted directly from the raw data segments. But FD features and DFC perform much better than TD, signifying the importance of transformed features in identifying SRF. The FD features give almost similar accuracy in both the datasets with the models, but an apparent discriminative ability can be determined with DFC features in the transformed domain. This shows that DFC contains more symptomatic fault features of SRF, with less complex extraction operation than traditional FD features. It is evident that all the three ML methods

provide the highest accuracy with DFC, especially the ANFIS model. The role of DFC as decision parameters of SRF is exploited by the rules derived by ANFIS, much better than the other models. This establishes DFC as the most dependable feature for SRF. Among the datasets, DS-2 got higher accuracy than DS-1, especially with TD features. But in the transformed domain, there is no significant performance enhancement for DS-2. ANN and SVM show almost similar performance for both datasets with a slight upper hand for ANN, while with the transformed data, ANFIS is dominating. From the discussion, It is apparent that DFC demonstrated its role in efficacious SRF diagnosis. The impact of DFC with sequential DL methods can be verified from section 4.5.2. These result leads to recognizing DFC as the main component of SRF diagnosis in the proposed framework.

3.6 Summary

In order to promote the fault-characteristics-based analysis of RM fault diagnosis, understanding the vibrational characteristics of the faults are very much essential. This chapter serves this purpose by providing the theoretical background of rotor faults with fault characteristics analysis. It also illustrates a general AI-based RFD framework, which we followed in all the models described in the remaining chapters. Similarly, data availability drives the recently developed intelligent data-driven methods. The RM fault diagnosis suffers from various data-related issues such as data scarcity, data imbalance, and impure data. Furthermore, it is indispensable that data must reflect real plant working environments. Hence, this chapter is provided a description of the datasets we used in the experiments. Similarly, this chapter emphasizes the role of DFC in SRF with the summarization of various related findings and with the experiments conducted in our works in this regard.

The critical difference between the DS-1 and DS-2 data sets is the variation of speed used to capture the data. The operating range of rotational frequency is almost

similar in both datasets, with an upper band RPM of 3600. DS-1 has five different RPM conditions and six faults, while DS-2 contains four fault conditions with around 50 different rotor speeds of varying other operating conditions. It summarizes that the DS-2 dataset is more diverse as compared to the DS-1 data set. But the run-up and run-down data provide distinguished fault diagnosis capabilities to DS-1, which is absent in DS-2. Moreover, DS-1 is more imbalanced than DS-2, which demands additional metrics like F1-score to ensure its performance. The performance comparison with the conventional TD and FD features and DFC features has been done on SVM, ANN, and ANFIS algorithms. The DFC produced apparent discriminative ability compared to the other two features, especially over the TD features in the transformed domain. Moreover, the role of DFC as decision parameters of SRF has been proven by the exceptional results produced by ANFIS, which exploits the rules derived from DFC. Thus the impact of DFC is showed in SRF diagnosis, and the result leads to recognizing DFC as the main component of SRF diagnosis in the proposed framework